Journal of Power Sources 269 (2014) 299–307

Contents lists available at ScienceDirect

Journal of Power Sources

journal homepage: www.elsevier.com/locate/jpowsour

Poly(methyl methacrylate–acrylonitrile–ethyl acrylate) terpolymer based gel electrolyte for $LiNi_{0.5}Mn_{1.5}O_4$ cathode of high voltage lithium ion battery

Ping Sun, Youhao Liao*, Huili Xie, Tingting Chen, Mumin Rao, Weishan Li*

School of Chemistry and Environment, Key Laboratory of Electrochemical Technology on Energy Storage and Power Generation of Guangdong Higher Education Institutes, Engineering Research Center of Materials and Technology for Electrochemical Energy Storage (Ministry of Education), South China Normal University, Guangzhou 510006, China

HIGHLIGHTS

- P(MMA–AN–EA) terpolymer based GPE was designed for $LiNi_{0.5}Mn_{1.5}O_4$ cathode of 5 V lithium ion battery.
- PEG significantly improves the uniform and interconnected structure of P(MMA–AN–EA) porous membrane.
- The GPE presents high ionic conductivity and compatibility with cathode and anode.
- $LiNi_{0.5}Mn_{1.5}O_4$ cathode using the developed GPE exhibits excellent cyclic stability.

ARTICLE INFO

Article history:
Received 19 March 2014
Received in revised form
18 June 2014
Accepted 2 July 2014
Available online 9 July 2014

Keywords:
Poly(methyl methacrylate–acrylonitrile–ethyl acrylate)
Porous polymer membrane
Gel polymer electrolyte
$LiNi_{0.5}Mn_{1.5}O_4$ cathode
High voltage lithium ion battery

ABSTRACT

A novel gel polymer electrolyte (GPE), based on poly(methyl methacrylate–acrylonitrile–ethyl acrylate) (P(MMA–AN–EA)) terpolymer, is designed to match $LiNi_{0.5}Mn_{1.5}O_4$ cathode of 5 V lithium ion battery. The performances of the synthesized P(MMA–AN–EA) terpolymer and the corresponding membrane and GPE are investigated by scanning electron microscope, energy dispersive spectroscopy, nuclear magnetic resonance spectra, Fourier transform infrared spectra, thermogravimetric analyzer, electrochemical impedance spectroscopy, linear sweep voltammetry, and charge/discharge test. It is found that the pore structure of P(MMA–AN–EA) membrane is affected by the dose of pore forming agent, polyethylene glycol (PEG400). The membrane with 3 wt% PEG400 presents the best pore structure, in which pores are dispersed uniformly and interconnected, and exhibits the largest electrolyte uptake, resulting in the highest ionic conductivity of 3.82×10^{-3} S cm^{-1} for the corresponding GPE at room temperature. The GPE has improved compatibility with lithium anode and is electrochemically stable up to 5.2 V (*vs.* Li/Li^+). The high voltage $LiNi_{0.5}Mn_{1.5}O_4$ cathode using the resulting GPE exhibits excellent cyclic stability, maintaining 97.9% of its initial discharge capacity after 100 cycles compared to that of 79.7% for the liquid electrolyte at 0.5 C.

1. Introduction

$LiCoO_2$ was adopted for the commercial lithium ion battery as the first generation of cathode by Sonny Company in 1990s. Researchers since then have been pursuing alternative cathodes due to the relatively low safety and the high cost of $LiCoO_2$. Spinel $LiMn_2O_4$ and olivine $LiFePO_4$ cathodes are then commercialized, but the low output voltage plateau of $LiMn_2O_4$ (3.9 V) and $LiFePO_4$ (3.2 V) cannot satisfy the target of developing higher power density of lithium ion battery. The most effective way is to promote the operation voltage of cathode materials. Thus, the $LiNi_{0.5}Mn_{1.5}O_4$ cathode has attracted more and more attentions because of its relatively high voltage platform of 4.7 V (versus Li/Li^+) and acceptably reversible capacity of about 130 mAh g^{-1} [1].

However, there are still some problems that need to be solved before the commercial application of $LiNi_{0.5}Mn_{1.5}O_4$ cathode in 5 V lithium ion battery. The major issue is the decomposition of carbonated organic liquid electrolyte at the voltage higher than 4.5 V, resulting from the oxidation of the free solvent components in organic electrolyte, such as ethylene carbonate (EC), dimethyl carbonate (DMC). Therefore, seeking a matched electrolyte for high voltage cathode is necessary.

* Corresponding authors. Tel./fax: +86 20 39310256.
E-mail addresses: liaoyouhao@126.com (Y. Liao), liwsh@scnu.edu.cn (W. Li).

http://dx.doi.org/10.1016/j.jpowsour.2014.07.014
0378-7753/

Avoiding the usage of the organic solvents, the solid electrolyte with high decomposed voltage is considered as the safest electrolyte in lithium ion battery. The exciting results, with regard to the inorganic solid electrolyte represented by Garnet-type [2] and LISICON (LIthium Super Ionic CONductor) structure [3], show that their ionic conductivity can be higher than 10^{-3} S cm^{-1} at room temperature. However, the problems of interfacial compatibility between solid electrode and solid electrolyte, the low mechanical strength and the poor flexible processibility, have become headaches when inorganic solid electrolyte is applied to the commercial battery. Poly(ethylene oxide) composites based solid polymer electrolyte has good processibility compared to inorganic solid electrolyte, but exhibits low ionic conductivity in the range of 10^{-8}–10^{-5} S cm^{-1} at room temperature, which is far lower than the commercial liquid electrolyte.

Gel polymer electrolyte (GPE), formed by swelling the organic liquid electrolyte into the suitable polymer matrixes [4,5], is a compromise of safe solid electrolyte with high electrochemical stability and liquid electrolyte with acceptable ionic conductivity at room temperature. The properties of matrix for GPE play a crucial role on the performances of GPE. Many polymers have been reported to be used as matrixes for GPE [6,7], including poly(-vinylidenefluoride) (PVDF) [8,9], polyacrylonitrile (PAN) [10], poly(methyl methacrylate) (PMMA) [11], and poly(ethylene oxide) (PEO) [12,13]. Unfortunately, the performances of currently available homopolymer in terms of mechanical strength, ionic conductivity and electrochemical stability cannot meet the requirement of commercial lithium ion batteries. For example, PMMA has good liquid electrolyte retention but poor mechanical behavior [14], PAN exhibits pleasant electrochemical stability but pathetic compatibility with lithium anode [15].

These drawbacks can be avoided, to some extent, by forming the copolymers through cross-linking or copolymerization with different functional monomers. Bi-polymers of poly(methyl methacrylate–acrylonitrile) (P(MMA–AN)) [16], poly(methyl methacrylate–vinyl acetate) (P(MMA–VAc)) [17], poly(-acrylonitrile–vinyl acetate) (P(AN–VAc)) [18], poly(butyl methacrylate–styrene) (P(BMA–St)) [19], and terpolymers of poly(methyl methacrylate–acrylonitrile–vinyl acetate) (P(MMA–AN–VAc)) [20], poly (acrylonitrile–methyl methacrylate–styrene) (P(AN–MMA–St)) [21], poly(methyl methacrylate–vinyl acetate)-*co*-poly(ethylene glycol) diacrylate (P(MMA–VAc)–PEGDA) [22] have been considered in our groups to be used as the matrixes of GPE. It is found that the comprehensive performances of terpolymer based GPE is much better than that of bi-polymer. Ethyl acrylate (EA) as a soft monomer exhibits good cohesiveness when applies for synthesizing the macromolecule [23].

In this paper, we report a new GPE based on terpolymer P(MMA–AN–EA) employing the MMA, AN and EA as monomers that designs for matching $LiNi_{0.5}Mn_{1.5}O_4$ cathode of 5 V lithium ion battery. P(MMA–AN–EA) is synthesized using the emulsion polymerization method while the membrane is obtained through phase inversion process with different doses of pore forming agent, polyethylene glycol (PEG400). The effects of PEG400 on the porous structure of P(MMA–AN–EA) membrane and electrochemical properties of corresponding GPE are investigated. The performance of the developed GPE is evaluated in the Li/GPE/$LiNi_{0.5}Mn_{1.5}O_4$ coin cell.

To our knowledge, the mechanical strength and ionic conductivity are the most important characterizations that determine the practical usage of the GPE, which are usually contradictory in fact. Although self-supported terpolymer P(MMA–AN–EA) based GPE may have higher electrolyte uptake and ionic conductivity, it should exhibit unsatisfied performance on the mechanical strength. In order to obtain the comprehensive performance of GPE, polyethylene (PE) separator was used as the support to ensure the mechanical strength of the GPE.

2. Experimental

2.1. Preparation

Commercial monomers MMA (>99.5%), AN (>99.5%) and EA (98.0%) were distilled in vacuum to remove the aggregation inhibitor. The synthesis of the P(MMA–AN–EA) terpolymer was conducted in a four neck glass reactor. 1.5 wt% sodium dodecyl sulfate (SDS, as an emulsifier) was dissolved in deionized water under N_2 at 60 °C. The mixture of monomer MMA, AN and EA with mass ratio of 4:2:1 was added into the SDS solution under stirring vigorously for 0.5 h to form the emulsified solution. 0.15 wt% sodium persulfate ($Na_2S_2O_8$, as an initiator) was slowly added into the emulsion within 0.5 h under stirring. After 6 h, the reaction was finished and the emulsion was poured into 2 wt% $Al_2(SO_4)_3$ solution to precipitate. Washed by the deionized water and ethanol, the P(MMA–AN–EA) terpolymer in the form of white powder was obtained by drying the precipitate in vacuum at 60 °C for 24 h.

The pore structure of membrane is closely related to its electrolyte uptake and electrochemical stability, and the interconnected pore structure will promote its comprehensive performance of corresponding GPE. Foaming agents such as salicylic acid, urea, are used for forming better pore structure according to the reports [24,25]. These porous membranes are obtained by heating the membrane to elevated temperature for several hours through the decomposition of the foaming agent. The complex process inspires us to find a simple and effective way to prepare the porous membrane. Therefore, PEG400 (polyethylene glycol, Molecular weight 400) is adopted as the pore forming agent for preparing the porous membrane.

The obtained P(MMA–AN–EA) terpolymer was dissolved at a concentration of 3 wt% in dimethylformamide (DMF) at 80 °C for 1 h and PEG400 with different mass ratios was added together with terpolymer. The resulting viscous slurry was cast with a doctor blade onto both sides of polyethylene (PE) separator, successively transferred into the sink surrounded by deionized water to induce phase inversion. The membrane was then rinsed with water and immersed into deionized water for 2 h in order to remove the residual solvent of DMF and PEG400 completely. Finally, the porous membrane was obtained by drying in vacuum at 60 °C for 24 h. For comparison, P(MMA–AN) membrane was also prepared.

The corresponding GPE was obtained by immersing the porous membrane into a liquid electrolyte of 1 M $LiPF_6$ in ethylene carbonate (EC)/dimethyl carbonate (DMC) (1:1, v/v, battery grade, Samsung Cheil Industry, Korea) for 0.5 h in an argon-filled glove box (Mbraun Unilab MB20, Germany). The final thickness of the GPE after coating double layers is 50 μm in average, while the thickness of PE support is 21 μm.

2.2. Characterization

The morphology of terpolymer powder was conducted on the scanning electron microscopy (SEM, ZEISS Ultra 55, Germany). Energy dispersive spectroscopy (EDS) was attached to the SEM instrument. Nuclear magnetic resonance (NMR) spectra of the terpolymer were measured in dimethyl sulphoxide (DMSO) solvent using Bruker AVANCE AV 400 MHz spectrometer. The structure of the terpolymer was also characterized by Fourier transform infrared (FTIR, Nicolet6700, USA) spectra in the range of 450–4000 cm^{-1}. The thermal stability of the copolymers was analyzed with thermogravimetric analyzer (TGA, Perkin–Elmer TGA7). The morphology of the resulting membranes was examined by SEM (JEOL, JSM-6510, Japan).

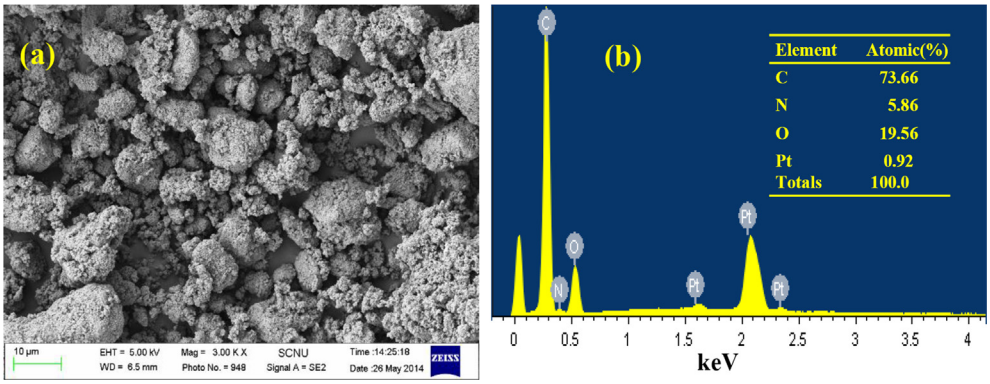

Fig. 1. (a) SEM image and (b) EDS spectra of P(MMA–AN–EA) terpolymer powder.

The electrolyte uptake (A) was calculated according to Eq. (1):

$$A(\%) = \frac{W_2 - W_1}{W_1} \times 100\% \quad (1)$$

where W_1 and W_2 were the mass of the dry and wet membranes, respectively.

The GPE was sandwiched between two parallel stainless steel (SS) discs (diameter Φ = 16.2 mm) and measured by electrochemical impedance spectroscopy (EIS) on electrochemical instrument (Metrohm Autolab PGSTAT302N, the Netherlands) using alternative current signal with potential amplitude of 10 mV and frequencies from 100 kHz to 1 Hz at various temperatures. The ionic conductivity (σ) was calculated from the bulk electrolyte resistance (R) according to Eq. (2):

$$\sigma = \frac{l}{RS} \quad (2)$$

where l was the thickness of the GPE, S the contact area between GPE and SS disc.

The interfacial stability was measured by sandwiching the GPE between two lithium electrodes. The Li/GPE/Li coin cell was conducted on Metrohm Autolab instrument (PGSTAT302N, the Netherlands) using alternative current signal with potential amplitude of 5 mV and frequencies from 500 kHz to 0.03 Hz. The oxidative stability of the GPE was examined in the coin cell with the structure of Li/GPE/SS by linear sweep voltammetry (LSV) at the scanning rate of 1 mV s^{-1} on Metrohm Autolab instrument as well. The SS was used as working electrode and the lithium as the reference and the counter electrodes.

Cathode electrode was fabricated by mixing the active material of $LiNi_{0.5}Mn_{1.5}O_4$, conductive agent of carbon black and binder of polyvinylidene fluoride (PVDF) in the weight ratio of 80:10:10. N-methylpyrrolidone (NMP) was applied as a solvent to prepare the electrode slurry. To determine the performance of $LiNi_{0.5}Mn_{1.5}O_4$ cathode in 5 V lithium ion battery using the resulting GPE, 2025 type coin cell Li/GPE/$LiNi_{0.5}Mn_{1.5}O_4$ was set up and tested on charging/discharging instrument (Land CT2001A, Wuhan Land Electronic Co. Ltd, China) between 3.5 V and 5.0 V at room temperature.

3. Results and discussion

3.1. Structure of terpolymer

Fig. 1(a) shows the SEM image of the prepared terpolymer powder, which is clustered round a lot of small sized particles. To determine whether precipitating agent $Al_2(SO_4)_3$ was completely removed in the terpolymer, EDS spectrum is carried out and the result is presented in Fig. 1(b). There is no characteristic peaks concerning about the Al or S element, which should be located in 2.69 keV and 2.07 keV in EDS spectrum, suggesting that $Al_2(SO_4)_3$ does not remain in the terpolymer. The embedded table in Fig. 1(b) indicates that the main element in terpolymer is C, N and O, which originates from the raw materials.

Fig. 2 presents the FTIR spectra of monomers, MMA, AN, EA, and their terpolymer P(MMA–AN–EA). The MMA shows its characteristic absorption at 1639.37 cm^{-1} and 1725.51 cm^{-1}, corresponding to C=C and C=O groups, respectively. The absorption peaks at 1608.57 cm^{-1} and 2228.95 cm^{-1} should be assigned to C=C and C≡N groups in AN monomer, while the absorption of C=C and C=O groups in EA monomer is reflected in 1637.29 cm^{-1} and 1726.30 cm^{-1}. Compared with the FTIR spectra of MMA, AN and EA monomer, the P(MMA–AN–EA) terpolymer keeps the main absorption peaks at 1727.65 cm^{-1} for C=O and the 2239.77 cm^{-1} for C≡N while loses the absorption of C=C groups in each monomers. It suggests that the terpolymer is formed by opening the double bonds of C=C but remaining the main functional groups in each monomer. The possible synthetic route is presented in Scheme 1.

Fig. 3 presents the NMR spectra of P(MMA–AN–EA) terpolymer. As can be observed from ^1H NMR spectrum in Fig. 3(a), α-methyl proton (CH_3) and the methylene proton (CH_2) on the main chain of terpolymer is in the range of around 1.0–1.4 ppm and 1.8–2.2 ppm, respectively. The proton in DMSO solvent has strong response at 2.5 ppm. The peak at 3.2–3.4 ppm is caused by the methylene

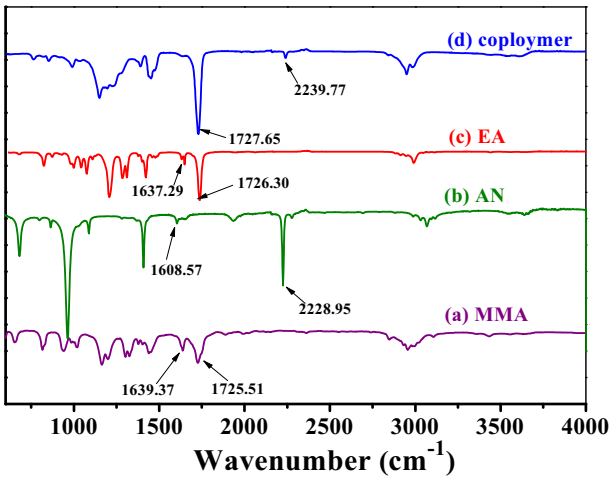

Fig. 2. FTIR spectra for monomers (a) MMA, (b) AN, (c) EA, and (d) their terpolymer P(MMA–AN–EA).

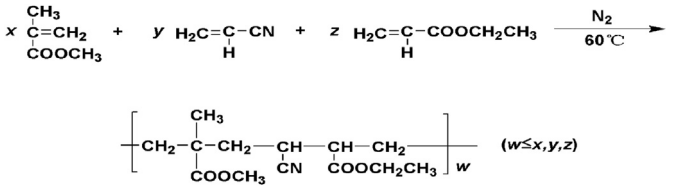

Scheme 1. The synthetic route of P(MMA–AN–EA) terpolymer prepared by emulsion polymerization.

proton (CH) connecting directly with cyanate carbon (C≡N) in terpolymer, which is ascribed to the AN unit [26,27]. The peak at around 3.6 ppm is due to the methoxy proton (O–CH_3) linked with nearby carbonyl group in the MMA chain [20]. The methylene proton (O–CH_2) of –OCH_2CH_3 chain segment in the EA unit is characterized at the peak of around 4.1 ppm [28]. In addition, there is no peak appearing at the range of 4.5–5.9 ppm, suggesting that alkenes proton (CH_2=C) does not exist in the terpolymer chains. The real monomer composition of MMA, AN and EA unit in the obtained terpolymer is calculated by the integral areas of each characterized proton peaks. The ratios of MMA, AN and EA in the obtained terpolymer chains is 4: 2: 0.68, in which the content of EA is smaller compared to ratios of 4: 2: 1 in raw materials, indicating that part of EA does not react. This unreacted EA has been removed totally through washing by deionized water and ethanol, which is proven by the loss of absorption peaks for C=C groups in terpolymer's FTIR spectrum and the absence of alkenes protons (CH_2=C) in ^{1}H NMR spectrum.

Fig. 3(b) is the ^{13}C NMR spectrum of terpolymer. The observed peak of methylene carbon (CH_2) is located at 27–29 ppm, the methine carbon (CH) at 33–34 ppm. The cyanate carbon (C≡N) related to AN unit is showed at 120 ppm, while the ester carbonyl carbon (O–C=O) in MMA and EA units is peaked at around 175 ppm [28]. However, the characteristic peak of alkenes carbon (CH_2=C) is not appeared at 100 ppm, which is in agreement with the result obtained by the FTIR and ^{1}H NMR spectra.

3.2. Thermal stability

The thermal stability of membrane is determined by TGA under N_2 atmosphere from room temperature to 600 °C at a heating rate of 10 °C min^{-1}. Here, the decomposition temperature is defined at losing its original weight larger than 5 wt%. It can be seen from Fig. 4 that TG curve of the P(MMA–AN–EA) membrane has similar shape but higher decomposed temperature than that of P(MMA–AN) membrane. P(MMA–AN) membrane is thermally stable up to 260 °C, while the decomposed temperature of P(MMA–AN–EA) membrane is as high as 315 °C. Apparently, adding the EA monomer

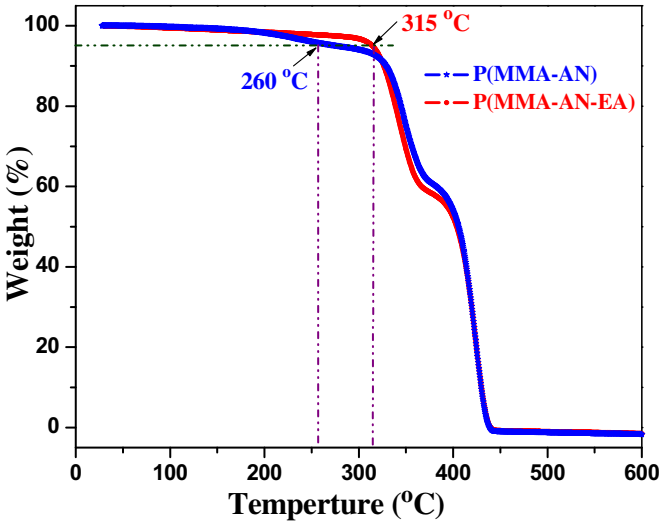

Fig. 4. TG curves of P(MMA–AN) and P(MMA–AN–EA) membranes.

to form P(MMA–AN–EA) terpolymer will hold back the decomposed rate of membrane during the heating process. The improvement in thermal stability results from the soft monomer of EA, which helps to enhance the crosslinked network structure in the terpolymer compared to bi-polymer.

3.3. Morphology of membranes

Pore structure of membrane determines its liquid electrolyte uptake and thus influences the properties of corresponding GPE. In order to obtain the high quality of porous membrane, PEG400 is selected as pore forming agent, which plays an important role on forming interconnected and uniformly distributed pore structure in the membranes. Fig. 5 presents SEM images of PE-supported P(MMA–AN–EA) membranes with different contents of PEG400. During the phase inversion process, the pore is formed by the exchange of solvent (DMF) and non-solvent (H_2O). It can be seen from Fig. 5(a) that a large number of un-uniform pores are distributed on the surface of P(MMA–AN–EA) membrane. After adding 1 wt% PEG400, the pores of membrane become uniform but not interconnected under the surface, as shown in Fig. 5(b). The improved porous structure can be observed when the content of PEG400 increases to 2 wt%, as shown in Fig. 5(c). The P(MMA–AN–EA) membrane with 3 wt% PEG400 exhibits best pore structure in the form of uniformly dispersed pores. The pore number on the surface is increased and the interconnected pores

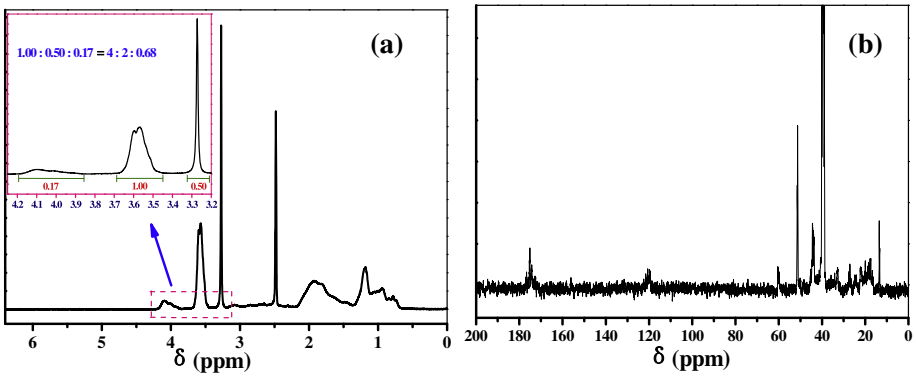

Fig. 3. (a) ^{1}H NMR and (b) ^{13}C NMR spectra of P(MMA–AN–EA) terpolymer.

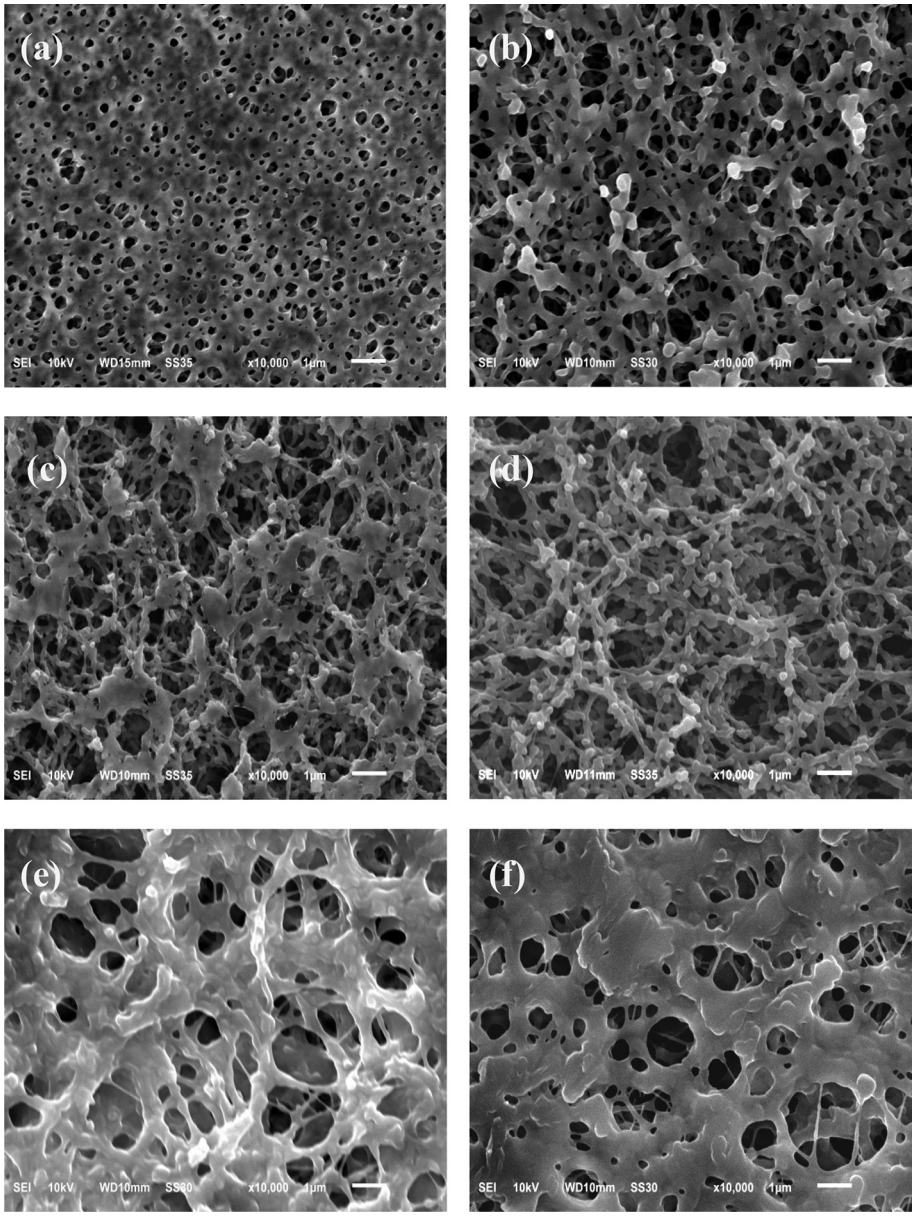

Fig. 5. SEM images of PE-supported P(MMA–AN–EA) membranes with different contents of PEG400, (a) 0 wt%, (b) 1 wt%, (c) 2 wt%, (d) 3 wt%, (e) 4 wt% and (f) 5 wt%.

under the surface can be seen clearly in Fig. 5(d). However, enhancing the content of PEG400 further, the pore size becomes extra large at the cost of interconnected porous structure, as shown in Fig. 5(e) and (f). During the phase inversion process, PEG400 is used as the secondary solvent phase, proper content (3 wt%) will benefit to form the suitable pore size in the membrane, while the less content is not enough to induce to form the interconnected pores. However, increasing the content of PEG400 further, the internal phase was quickly divided into the PEG400-rich and PEG400-poor phase caused by the different evaporated rate of DMF and PEG400, and the bigger pores are formed subsequently when the excess PEG400 is accumulated to a certain extent.

3.4. Electrolyte uptake

Fig. 6 presents the dependence of the electrolyte uptake for PE-supported P(MMA–AN–EA) membranes on the content of PEG400. It can be seen that the uptake of the membranes is closely related to the content of PEG400. The uptake of membrane without PEG400 is 102% according to Eq. (1), and the value increases as enhancing the content of PEG400, reaching the maximum level of 155% when the PEG400 content is 3 wt%, but declines with increasing the content of PEG400 further.

Based on the SEM observations (Fig. 5), it can be known that the electrolyte uptake depends greatly on its pore structure. The pore size of the membrane without PEG400 is too small to retain enough liquid electrolyte, resulting in the low electrolyte uptake. As the content of PEG400 increases, the pores in P(MMA–AN–EA) membrane become uniform and interconnected, leading to the enhancement in the ability for electrolyte uptake. The largest electrolyte uptake for the membrane should be ascribed to its improved pore structure. However, the pore size becomes too large to retain the liquid electrolyte effectively and the pore number is also reduced when the content of PEG400 increases further, resulting in the lowest electrolyte uptake.

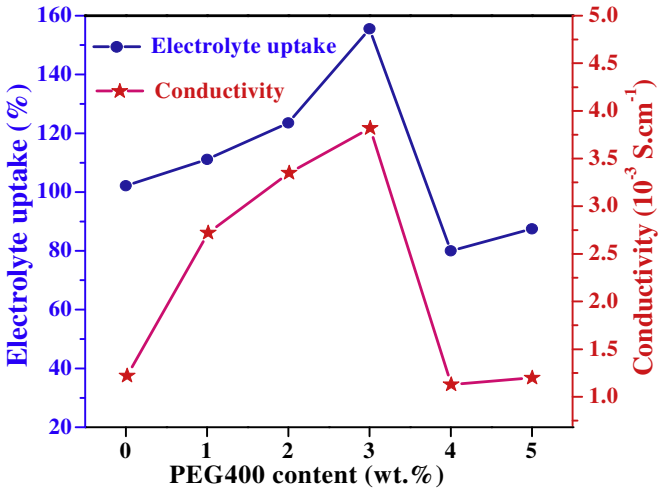

Fig. 6. The dependence of electrolyte uptake and ionic conductivity of P(MMA–AN–EA) based GPEs on the content of PEG400.

3.5. Ionic conductivity

Fig. 7 presents the Nyquist plots of the GPEs using P(MMA–AN–EA) as polymer matrix with different contents of PEG400 at room temperature. The ionic conductivity (σ) of GPE calculated by Eq. (2) was also presented in Fig. 6. At room temperature, $\sigma = 1.22 \times 10^{-3}$ S cm^{-1} is observed for P(MMA–AN–EA) based GPE without using PEG400. However, it reaches the largest value of 3.82×10^{-3} S cm^{-1} after adding 3 wt% PEG400, which is comparable to the liquid electrolyte in commercial lithium ion battery.

It also can be seen from Fig. 6 that the ionic conductivity of GPEs is proportional to their electrolyte uptakes, which is depended greatly on its pore structure. A large number of uniform and interconnected pores not only enlarge the contact areas between polymer and liquid electrolyte, but also help to retain the liquid electrolyte effectively by the special polymer–solvent interactions due to the existence of the strong polarity groups C≡N and C = O in the terpolymer matrix [29]. With these results, the better porous structure of membrane with 3 wt% PEG400 was chosen for further investigation.

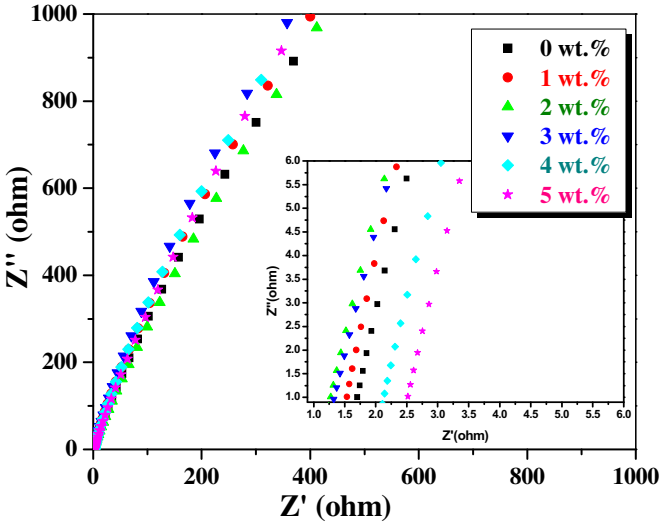

Fig. 7. The Nyquist plots of the P(MMA–AN–EA) based GPEs with different contents of the PEG400 using the cells of SS/GPE/SS at room temperature.

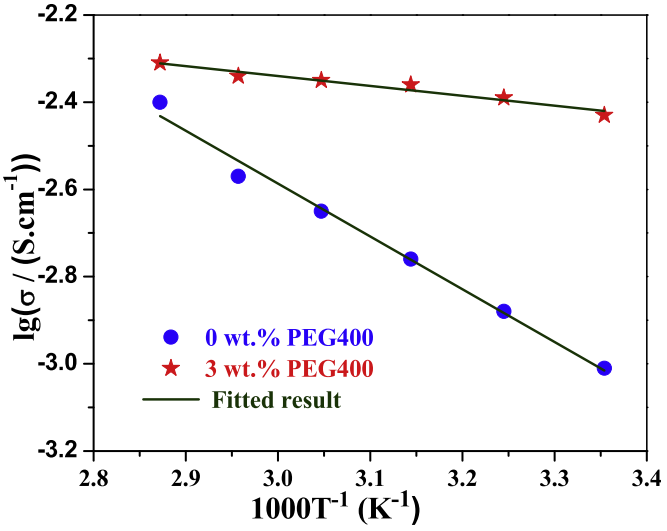

Fig. 8. Absolute temperature dependence of ionic conductivity for the GPEs using 0 wt % and 3 wt% PEG400.

To understand the conductivity mechanism of the GPEs without and with 3 wt% PEG400, the ionic conductivity is measured at the different temperatures. It can be seen from Fig. 8 that the conductivity increases with the absolute temperature in a linear relationship, exhibiting the same dependence on the reciprocal value of temperature for the various GPEs. This indicates that the conductive mechanism follows the Arrhenius law, and adding PEG400 to form different pore structure will not change the conductive mechanism of the P(MMA–AN–EA) based GPE.

The activation energy (E_a) of the GPEs for the lithium ion transfer is obtained from the Arrhenius plots of

$$\sigma_{Li} T = A \exp(-E_a/kT) \quad (3)$$

where σ was the ionic conductivity, T the absolute temperature, A the pre-exponential constant and k the Boltzmann constant.

E_a is 4.34 kJ mol^{-1} for the P(MMA–AN–EA) based GPE with 3 wt % PEG400, calculated from the slope of the fitting lines in the temperature range of 348 K–298 K, which is much lower than that of GPE without PEG400, whose value of E_a is as high as 23.17 kJ mol^{-1}. The lower E_a is a reflection of a lower barrier for the diffusion and migration of lithium ion, which can be ascribed to its uniformly distributed and interconnected pore structure.

3.6. Compatibility with anode

The compatibility of GPE with lithium anode was understood by the interfacial behavior of a lithium electrode in prolonged contact with a GPE, which was associated with the passive layer and the charge transfer resistances on the lithium electrode. The spectra are in the form of depressed semicircle intercepted with the real axis, and its diameter of semicircle reflects the electrode/electrolyte interfacial resistance (R_i) [30]. The R_i of the coin cells Li/GPE/Li are surveyed for various GPEs and the obtained results are presented in Fig. 9. It can be seen from Fig. 9(a) that the R_i for the poor pore structure based GPE without PEG400 increases from 69 Ω cm^2 on the first day to 86 Ω cm^2 after the 15 days. However, much lower increased magnitude can be observed for the GPE with 3 wt% PEG400, a negligible increase from 62 Ω cm^2 initially to 69 Ω cm^2 after the 15 days. The increased value at the beginning is attributed to the formation of a passive layer due to the interfacial reaction between GPE and lithium electrode. Maintaining the constant value

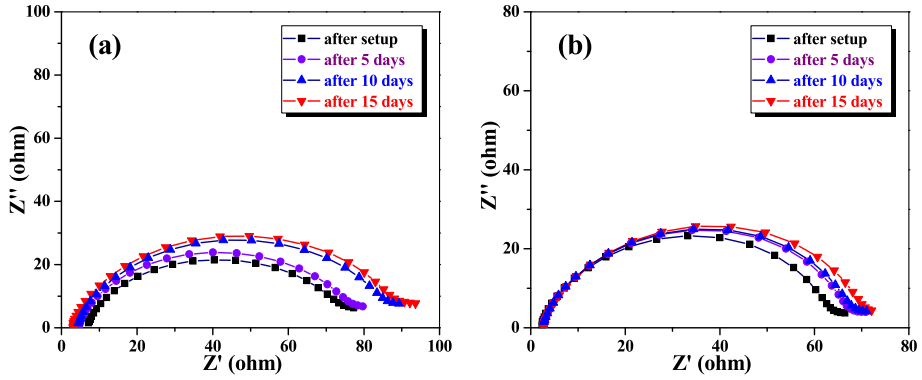

Fig. 9. Electrochemical impedance spectra of the cells Li/GPE/Li (a) without and (b) with 3 wt% PEG400.

for R_i as increasing the storage time is a reflection of the slowly interfacial reaction. The reason for the improved compatibility of GPE with lithium anode should be ascribed to the lower activity of liquid electrolyte by encapsulating into the polymer matrix, while this effect is strengthened after using the uniformly distributed and interconnected membrane by holding efficiently the liquid electrolyte in the polymer matrix.

3.7. Compatibility with cathode

For the practical usage in 5 V lithium ion battery, the compatibility of GPEs with cathode is crucial, which can be understood by their oxidative stability on stainless steel under anodic oxidation. The obtained results for various electrolytes are shown in Fig. 10. For comparison, the PE separator saturating the liquid electrolyte and the P(MMA–AN–EA) dry membrane are also sandwiched in Li/SS type coin cell to evaluate their oxidative stability. The PE separator with liquid electrolyte is decomposed at the potential of 4.4 V (*vs.* Li/Li^+) due to the oxidative reaction of the free solvent components in organic electrolyte. P(MMA–AN–EA) dry membrane without liquid electrolyte, however, has no current response in the whole scanning range, suggesting that P(MMA–AN–EA) itself has highly oxidative stability.

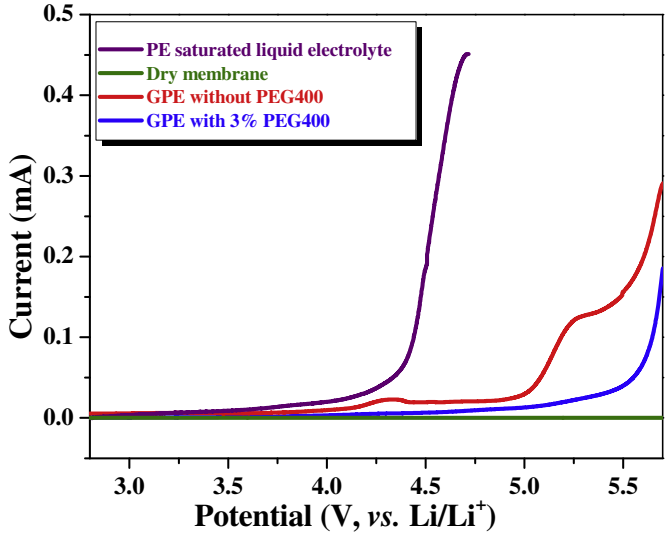

Fig. 10. Linear sweep voltammograms on stainless steel for PE separator saturated liquid electrolyte, P(MMA–AN–EA) dry membrane and P(MMA–AN–EA) based GPEs without and with 3 wt% PEG400, scanning rate: 1 mV s^{-1}.

The P(MMA–AN–EA) based GPEs exhibit better compatibility with cathode compared to the liquid electrolyte. As presented in Fig. 10, the P(MMA–AN–EA) based GPE is electrochemically stable up to 5.0 V (*vs.* Li/Li^+), while the GPE with better pore structure induced by 3 wt% PEG400 has the highest oxidative potential of 5.2 V (*vs.* Li/Li^+), indicating that the improved porous structure will not sacrifice the electrochemical stability of the GPE. Since the abundant pores accommodate a big amount of liquid electrolyte, the contact between the electrolyte and the cathode is good. Some of the electrolyte compositions existing on the membrane surface will directly contact with the cathode, bringing about the decomposition of the GPEs when the oxidative potential is higher than 5.0 V, which resulted from the oxidation of liquid components. The situated environment of liquid electrolyte determines different decomposed potential. After gelation the liquid electrolyte into the P(MMA–AN–EA) polymer matrix, the mobility of free liquid electrolyte is restricted and the activated reaction of organic electrolyte is reduced subsequently by the interaction between polymer matrix and liquid electrolyte through gelatinization process. The liquid electrolyte is less activated even if it stores in the pores of membrane and gelled polymer, leading to the enhancement in the compatibility with cathode. The improved oxidative stability of the developed GPE qualifies the better performance for high voltage cathode based lithium ion battery.

3.8. High voltage cathode performance

The characterization at high voltage is evaluated by using the developed GPE and 5 V $LiNi_{0.5}Mn_{1.5}O_4$ cathode. Fig. 11 shows the discharge curves of $LiNi_{0.5}Mn_{1.5}O_4$ cathode at different rates, which is charged at 0.1 C first, and then discharged at 0.1 C, 0.2 C, 0.5 C and 1 C gradually. As shown in Fig. 11, the voltage plateau and the discharge capacity decrease slowly as increasing the discharge rate but still keep relatively high values. The $LiNi_{0.5}Mn_{1.5}O_4$ achieves a capacity of 121.4 mAh g^{-1} at 0.1 C and 0.2 C (theory capacity extracted one Li: 146.7 mAh g^{-1}), and maintains 98.8% and 92.2% of its 0.1 C discharge capacity when discharged at 0.5 C and 1 C, respectively. The result indicates that the developed GPE exhibits suitable rate capability for the high voltage lithium ion battery use. The acceptable rate capability can be ascribed to the high ionic conductivity of the developed GPE, which is closely related to the uniformly distributed and interconnected pore structure.

Fig. 12 presents the cyclic stability of $LiNi_{0.5}Mn_{1.5}O_4$ cathode using the developed GPE, which is charged and discharged in the voltage ranges of 3.5 V–5.0 V at a constant current of 0.2 C and 0.5 C rate under room temperature, respectively. The detailed information on the charged and discharged curves for the selected 1st, 25th, 50th, 75th and 100th cycles of $LiNi_{0.5}Mn_{1.5}O_4$ cathode under

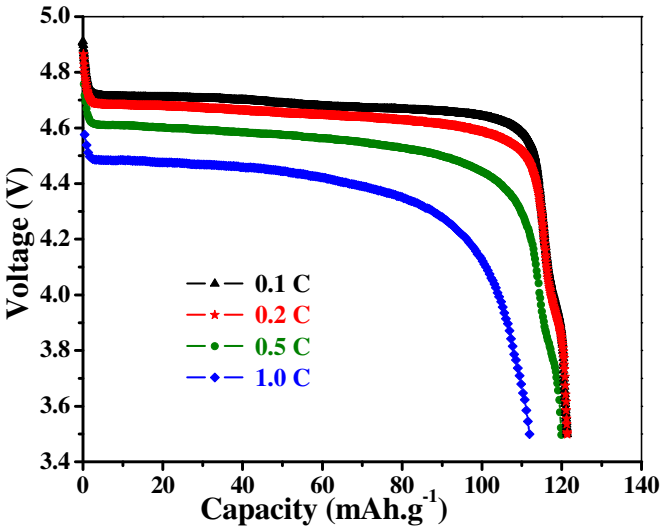

Fig. 11. Rate discharge curves of $LiNi_{0.5}Mn_{1.5}O_4$ cathode using the developed GPE.

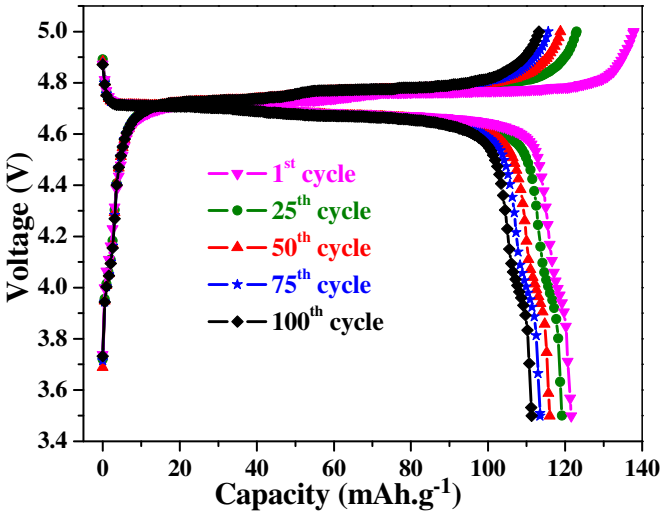

Fig. 13. Charge/discharge curves of the $LiNi_{0.5}Mn_{1.5}O_4$ cathode using the developed GPE for the 1st, 25th, 50th, 75th and 100th cycle at 0.2 C rate between 3.5 V and 5.0 V.

0.2 C is presented in Fig. 13. The voltage plateau at about 4.7 V (*vs.* Li/Li^+), which is a characteristic of spinel $LiNi_{0.5}Mn_{1.5}O_4$, is quite stable and almost unchanged with cycling, confirming the good compatibility of GPE with high voltage cathode and lithium anode. For comparison, the cyclic stability of the $LiNi_{0.5}Mn_{1.5}O_4$ cathode using the liquid electrolyte at different rates is also presented in Fig. 12. The capacity retention of the cathode combined with GPE is always higher than that with the liquid electrolyte after 100 cycles. Although the cathodes using various electrolytes have almost the same initial capacity of about 120 mAh g^{-1} at 0.2 C and 0.5 C, the capacity retention is different, 92.2% and 97.9% for the developed GPE at 0.2 C and 0.5 C, while only 79.7% and 82.7% for the liquid electrolyte after 100 cycles. Thus, developed GPE does improve the cyclic stability of the 5 V $LiNi_{0.5}Mn_{1.5}O_4$ cathode. To understand the GPE's binding strength between PE support and terpolymer, we disassemble the cycled coin cell. The result shows that the GPE keeps its original morphology after 100 cycles at 0.2 C rate, indicating the good binding strength between PE and terpolymer.

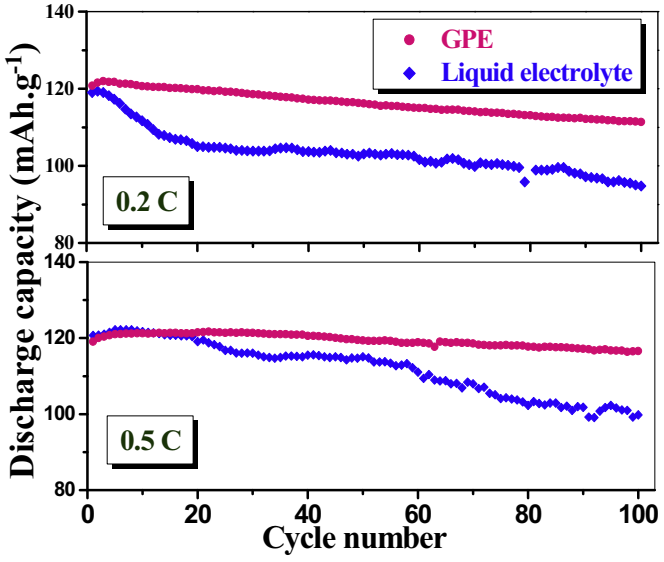

Fig. 12. Cyclic stability of the $LiNi_{0.5}Mn_{1.5}O_4$ cathode with various electrolytes under 0.2 C and 0.5 C rate in the voltage range of 3.5 V and 5.0 V at room temperature.

The main issue for applying $LiNi_{0.5}Mn_{1.5}O_4$ cathode in commercial lithium ion battery is the decomposition of liquid electrolyte that usually takes place at the operation voltage lower than 4.5 V. The suitable rate capability and the excellent cyclic stability provided by the prepared GPE makes the developed GPE become a bright alternative to organic liquid electrolyte for matching $LiNi_{0.5}Mn_{1.5}O_4$ cathode as well as other high voltage cathodes of 5 V lithium ion batteries.

4. Conclusions

A new gel polymer electrolyte (GPE), based on poly(methyl methacrylate–acrylonitrile–ethyl acrylate) (P(MMA–AN–EA)) terpolymer, is successfully developed for $LiNi_{0.5}Mn_{1.5}O_4$ cathode of 5 V lithium ion battery. Polyethylene glycol (PEG400) as the pore forming agent improves significantly the pore structure of P(MMA–AN–EA) membrane, and 3 wt% of PEG400 is the optimal content to develop a membrane with uniformly distributed and interconnected pore structure. The developed GPE based on P(MMA–AN–EA) membrane resulting from using 3 wt% of PEG400 exhibits improved electrolyte uptake and ionic conductivity at ambient temperature. The GPE also presents compatibility with anode and cathode of lithium ion battery, subsequently the $LiNi_{0.5}Mn_{1.5}O_4$ cathode using the GPE shows excellent cyclic stability. Therefore, the developed GPE provides an alternatively matched electrolyte for $LiNi_{0.5}Mn_{1.5}O_4$ cathode as well as other high voltage cathodes of 5 V lithium ion batteries.

Acknowledgments

The authors are highly grateful for the financial support from the joint project of National Natural Science Foundation of China and Natural Science Foundation of Guangdong Province (Grant No. U1134002), National Natural Science Foundation of China (Grant No. 21273084), Natural Science Foundation of Guangdong Province (Grant No. 10351063101000001, S2013040016471), China Postdoctoral Science Foundation funded project (Grant No. 2013M530369), the key project of Science and Technology in Guangdong Province (Grant No. 2011A010802001), and the scientific research project of Department of Education of Guangdong Province (Grant No. 2013CXZDA013).

References

[1] H.Y. Xu, S. Xie, N. Ding, B.L. Liu, Y. Shang, C.H. Chen, Electrochim. Acta 51 (2006) 4352–4357.
[2] Y. Li, J.T. Han, C.A. Wang, H. Xie, J.B. Goodenough, J. Mater. Chem. 22 (2012) 15357–15361.
[3] N. Kamaya, K. Homma, Y. Yamakawa, M. Hirayama, R. Kanno, M. Yonemura, T. Kamiyama, Y. Kato, S. Hama, K. Kawamoto, A. Mitsui, Nat. Mater. 10 (2011) 682–686.
[4] Q. Xiao, X. Wang, W. Li, Z. Li, T. Zhang, H. Zhang, J. Memb. Sci. 334 (2009) 117–122.
[5] J.Y. Song, Y.Y. Wang, C.C. Wan, J. Power Sources 77 (1999) 183–197.
[6] J.L. Shi, L.F. Fang, H. Li, H. Zhang, B.K. Zhu, L.P. Zhu, J. Memb. Sci. 437 (2013) 160–168.
[7] Q. Lu, J. Fang, J. Yang, R. Miao, J. Wang, Y. Nuli, J. Memb. Sci. 449 (2014) 176–183.
[8] Y. Zhu, S. Xiao, Y. Shi, Y. Yang, Y. Hou, Y. Wu, Adv. Energy Mater. 4 (2014) 1–9.
[9] Y. Zhu, F. Wang, L. Liu, S. Xiao, Z. Chang, Y. Wu, Energy Environ. Sci. 6 (2013) 618–624.
[10] B. Huang, Z. Wang, L. Chen, R. Xue, F. Wang, Solid State Ionics 91 (1996) 279–284.
[11] Y. Wang, X. Ma, Q. Zhang, N. Tian, J. Memb. Sci. 349 (2010) 279–286.
[12] L.F. Fang, J.L. Shi, B.K. Zhu, L.P. Zhu, J. Memb. Sci. 448 (2013) 143–150.
[13] Q. Lu, J. Fang, J. Yang, G. Yan, S. Liu, J. Wang, J. Memb. Sci. 425–426 (2013) 105–112.
[14] M. Rao, X. Geng, Y. Liao, S. Hu, W. Li, J. Memb. Sci. 399-400 (2012) 37–42.
[15] D.Y. Zhou, G.Z. Wang, W.S. Li, G.L. Li, C.L. Tan, M.M. Rao, Y.H. Liao, J. Power Sources 184 (2008) 477–480.
[16] M.M. Rao, J.S. Liu, W.S. Li, Y. Liang, D.Y. Zhou, J. Memb. Sci. 322 (2008) 314–319.
[17] L. Lu, X.X. Zuo, M.Q. Xu, J.S. Liu, W.S. Li, Acta Chim. Sin. 65 (2007) 475–480.
[18] X.P. Li, M.M. Rao, Y.H. Liao, W.S. Li, M.Q. Xu, J. Appl. Electrochem 40 (2010) 2185–2191.
[19] Y.H. Liao, M.M. Rao, W.S. Li, L.T. Yang, B.K. Zhu, R. Xu, C.H. Fu, J. Memb. Sci. 352 (2010) 95–99.
[20] Y.H. Liao, D.Y. Zhou, M.M. Rao, W.S. Li, Z.P. Cai, Y. Liang, C.L. Tan, J. Power Sources 189 (2009) 139–144.
[21] L. Chen, M.M. Rao, W.S. Li, M.Q. Xu, Y.H. Liao, C.L. Tan, J. Yi, Acta Phys. Chim. Sin. 27 (2011) 1689–1694.
[22] Y.H. Liao, X.P. Li, C.H. Fu, R. Xu, M.M. Rao, L. Zhou, S.J. Hu, W.S. Li, J. Power Sources 196 (2011) 6723–6728.
[23] O. Quadrat, J. Snuparek, J. Mikesova, J. Horsky, Colloid. Surf. A 253 (2005) 163–168.
[24] H.P. Zhang, P. Zhang, G.C. Li, Y.P. Wu, D.L. Sun, J. Power Sources 189 (2009) 594–598.
[25] Z.H. Li, C. Cheng, X.Y. Zhan, Y.P. Wu, X.D. Zhou, Electrochim. Acta 54 (2009) 4403–4407.
[26] Z.L. Wang, Z.Y. Tang, Electrochim. Acta 49 (2004) 1063–1068.
[27] W.H. Pu, X.M. He, L. Wang, Z. Tian, C.Y. Jiang, C.R. Wan, Ionics 14 (2008) 27–31.
[28] E. Vargün, M. Sankır, A. Usanmaz, Y. Kanbur, U. Abacı, H.Y. Güney, J. Appl. Polym. Sci. 124 (2012) 840–846.
[29] J.Y. Kim, Y. Lee, D.Y. Lim, Electrochim. Acta 54 (2009) 3714–3719.
[30] Y.B. Fu, X.H. Ma, Q.H. Yang, X.F. Zong, Mater. Lett. 57 (2003) 1759–1764.